Poole, D., Bevan, R., Allen, C., & Rendall, T. (2016). An Aerodynamic Model for Vane-Type Vortex Generators. In 8th AIAA Flow Control Conference (AVIATION2016). [AIAA 2016-4085] American Institute of Aeronautics and Astronautics Inc, AIAA. DOI: 10.2514/6.2016-4085

An Aerodynamic Model for Vane-Type Vortex Generators

D.J. Poole [*], R.L.T. Bevan [†], C.B. Allen [‡], T.C.S. Rendall[§]

Department of Aerospace Engineering, University of Bristol, Bristol, BS8 1TR, U.K.

A new, physics-based model is presented for flows around vortex generators. The model uses a modified lifting-line method with added physics to account for boundary layer flow. The lifting-line method is extended to also include a vortex lift component and these two components are used to calculate the strength of a vortex shed from an isolated vortex generator. The circulation model is developed further to be used within a CFD framework in a source term approach. Validation is presented, first for the circulation model against a suite of experimental tests for isolated vortex generators where the vortex strength is measured. Excellent agreement is shown that is of the order of the experimental error; 5%. Second, the source term model is validated on a flat plate mounted vortex generator problem, and compared to fully-gridded simulations and the commonly used Bender-Anderson-Yagel model. Again, the new method shows excellent agreement, matching well the circulation decay and velocities downstream of the VG.

I. Introduction

During the latter design phases of aircraft it is common for unwanted flow phenomena to arise that were not predicted in the original design, and hence it can be common to add flow control devices to aircraft to alter the flowfield in specific regions. Occasionally, complex active systems have been implemented to control boundary layer growth, including boundary layer suction, blowing, and bleeding, but by far the most common methods are passive schemes, with vortex generators (VGs) the most conventional approach.[1,2,3,4] These generally involve simple small plates mounted normal to the surface, usually rectangular in shape, inclined to the freestream flow. An example is the use of VGs on the Bell XV-15.[5] The majority of VGs protrude into the external flow, i.e. above the boundary layer, but there have also been immersed, or sub-layer, VGs adopted.[6]

VGs are predominantly used to mitigate against separated flows (although can also be used to delay transition[7]), and are placed a distance upstream of where the separation occurs to suitably re-energise the boundary layer to avoid the separation. Vortical flow is introduced via the flow separation from its sharp upper edge, and the vortex which subsequently propagates downstream entrains higher energy, higher momentum flow from outside the boundary layer into the lower energy boundary layer. This re-energises the boundary layer, suppressing separation.

It is necessary to understand the physics that the VGs are introducing into the flow to be able to design them to mitigate against unwanted flow phenomena (e.g. separation). In recent years, computational fluid dynamics (CFD) has become a standard tool for aircraft design, however, modelling of VGs by conventional CFD approaches poses difficult issues in capturing the vortex and its convection downstream. This often requires fine numerical meshes on geometries where the size of the flow control device is orders of magnitude smaller than the global object. Furthermore, a sufficiently high fidelity numerical scheme must be selected, usually requiring RANS solutions with turbulence models, leading to difficult numerical challenges.

Modelling issues, along with the notion that often VGs are added as an after-design modification, mean that using CFD to predict VG flow can cause bottlenecks late in the development process. To alleviate some

[*]Graduate Student. Email: d.j.poole@bristol.ac.uk

[†]Research Assistant. Email: r.bevan@bristol.ac.uk

[‡]Professor of Computational Aerodynamics. Email: c.b.allen@bristol.ac.uk

[§]Lecturer. Email: thomas.rendall@bristol.ac.uk

of these issues, while still maintaining the physical fidelity required to accurately model the flow around VGs, a source term approach within a CFD framework can be adopted. This involves a forcing term added to specific cells within the numerical domain to mimic the effect of a VG being present, though without the need to model the VG itself. The most common example is the Bender-Anderson-Yagel (BAY) model.[8]

While the BAY model is an effective tool for VG flows, implementation of it can cause problems. Hence, the work presented in this paper details the development of a new model to allow rapid integration into the CFD process. A circulation model is developed from a lifting-line formulation, with added physical modifications made to account for the boundary layer flow and the effect of the vortex on the overall lift of the VG. This circulation approximation model is validated against experimental data. The source term model is then developed and compared to the BAY model and fully-gridded CFD on a flat plate test, and also compared to experimental data.

II. Methods of Modelling Vortex Generators

The physics of a flowfield when a vortex generator (VG) is placed into the flow differs considerably from a clean geometry. The VG produces a vortex which encourages mixing of turbulent flow downstream of the device, often used to avoid unwanted separation. The exact physics of flow control using VGs is complicated, however, there tends to be three fidelities of physics in models used to simulate VG behaviour:

1. **High fidelity physics**: Full iterative CFD simulation with fine computational meshes;
2. **Medium fidelity physics**: Iterative simulation but with a term to mimic the effect of the VG;
3. **Low fidelity physics**: Analytical model without the need for iterative solutions.

II.A. High Fidelity Physics

The highest fidelity simulations for modelling VG behaviour are by conventional CFD approaches. This modelling approach first requires a body-fitted mesh to be placed around the aerodynamic surface of interest. Difficulties tend to arise in the meshing due to the large differences in scale that exist between the parent geometry and the flow control device. Furthermore, to effectively capture and convect downstream the vortex produced by the device, fine resolution grids are often required around the VG and in its wake, resulting in the exponential growth of mesh sizes when compared to a clean wing counterpart.

The solution of the flowfield usually requires at least RANS simulations with a turbulence model to be performed. The effective capture of the viscous effects are imperative to ensure modelling of the shed vortex, and therefore its effect downstream. Examples of typical simulations for flow around VGs using conventional CFD methods include.[9,10,11,12,13,14]

To fully capture all the flow physics associated with the VG, very high-fidelity, real-time, simulations via large eddy simulation (LES) or direct numerical simulation (DNS) methods are required, though these tend to be prohibitively expensive for use in the design phase. As such, historically it has been difficult to perform such simulations for large Reynolds numbers, however, with the continual increase in computational resources available these are becoming more common.[15,16,17] The Lattice-Boltzmann method[18] has also been used to produce time-dependent flow simulations around VGs.[19]

II.B. Medium Fidelity Physics

Often great effort must be expended in terms of mesh generation and computational resources for high-fidelity CFD methods to be able to capture, sufficiently, the convection of the physical quantities associated with flow around VGs. One possible way to overcome the issues associated with meshing comes from recognising that the mesh issues originate from requiring an extrusion on the surface that is orders of magnitude smaller than the global object. Therefore, if the requirement for meshing around this small object is removed, then this makes the meshing process simpler, and this idea is the basis behind modelling the effect of the VG instead of the actual VG itself.

This, medium fidelity, approach uses source terms to create a disturbance where the VG would otherwise exist. The three common approaches are by adding either a vortex source[20,21] term, or a lifting-force[8,22,23] term or a statistical[24] term, which are added at cells in the computational domain close to where the VG

would be. The solution then proceeds by a traditional CFD numerical approach. By eliminating the physical VG, the meshing requirements are somewhat relaxed, usually leading to smaller meshes.

A notable method for modelling VGs using a medium fidelity physics model is that of Kerho and Kramer[25] who modified the aerofoil simulation and design tool XFOIL,[26,27] to mimic the effect that VGs have of producing turbulence within the boundary layer to mitigate against separation. Their modification involved adding turbulence at the site of a VG by modifying the stress transport equation. While this method does not strictly allow for the full three-dimensional effects of the shed vortex, it still acts as a useful trade-off design tool for VG design.

II.C. Low Fidelity Physics

The requirement to capture and convect the necessary physics downstream necessitates, still, the need for fine enough meshes, even when using medium fidelity simulation approaches. To eliminate this requirement, an option is to use a simpler, often analytical modelling approach. These types of models are the lowest fidelity simulation approach that can feasibly be done to obtain the effects of VGs on the flowfield.

The simplest method is a pure lifting-line approach, where the VG is modelled as a wing in uniform oncoming flow, and lifting line theory is used to capture the strength of the shed vortex. Lamb vortices are then commonly used to model the effects of the vortex on the flowfield. A second method is due to Wendt[28] which is an empirical model. A least squares fit of a large set of experimental results is used to obtain a lifting-line type equation for the vortex strength, but with modifications made from observations of the empirical fit to account for the boundary layer. The vortex is then modelled using the Lamb vortex model to obtain the effect of the vortex on the flowfield. The Wendt model has also been implemented in the NASA Wind-US solver[29] as a vortex-source term (medium fidelity approach), with reasonable agreement being shown between the CFD with source term and experimental data.

II.D. Problem Considered

The source term approach is a commonly used method for VG flows, and provides a good balance between higher-fidelity physics, yet smaller meshes and therefore cheaper solutions. These models tend to be based around approximating the VG as a simple wing, similar to the models of Prandtl and Wendt, which do provide a good trade-off between accuracy and speed for determining the effect of a VG, however, as will be shown later, both these models lack extra physics associated with flows around VGs that can be added using extra analytical terms.

This has driven the development of a new source term model, which has a simple-to-compute source term, however yields results with more physical meaning. The method is constructed around the conventional source-term framework so still maintains the simplicity of other methods.

III. Modified Lifting-Line for Vortex Strength

A VG can be modelled as a lifting wing, albeit a very small wing with a low aspect ratio. As such, lifting-line theory can be used to approximate the strength of the vortex shed from the tip of the VG (which can be thought of as the tip of the wing represented by the VG). The lifting-line theory is described below followed by the application of the theory to VGs and the modifications made to it to ensure it is more suitable for the nature and scale of VGs.

III.A. Lifting-Line Theory

The development of a model used to simulate the strength of a vortex shed from a VG is driven from Prandtl's lifting-line theory.[30] The VG is modelled as a lifting wing with a single shed vortex. Lifting-line can then approximate the strength of the shed vortex. It should be noted that strictly, lifting-line theory assumes long and slender wings, hence for VGs, which often have a very low aspect ratio, the assumptions in this theory are at the limit of acceptability. As the model only needs to be an approximation of the effect of the vortex, the use of a lifting-line is suitable. 7 The important elements of lifting-line theory as pertaining to the development of the analytical model are outlined below. Full discussions of lifting-line theory and its applications to aircraft design are outlined by, for example, Glauert[31] and Pope.[32]

The spanwise location along a wing of semi-span s, as shown in figure 1[a] is transformed into a trigonometric formulation by letting $y = -s\cos\theta$, hence the spanwise location of the wing is now described in terms of θ, so $0 \leq \theta \leq \pi$.

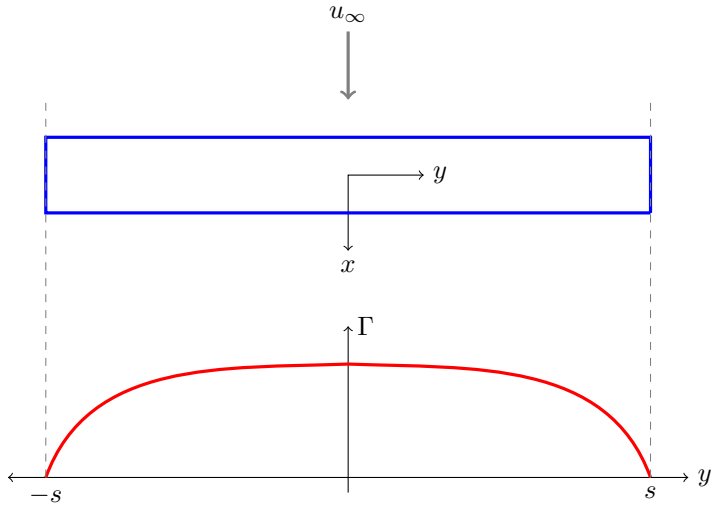

Figure 1: Lifting-line wing geometry

A symmetrical circulation distribution Γ (shown in figure 1) over the wing is described by an infinite Fourier series using only sine functions:

$$\Gamma = 4su_\infty \sum_{n=1}^{\infty} A_n \sin(n\theta) \tag{1}$$

where u_∞ is the freestream velocity and A_n is the n-th Fourier coefficient. At a particular point on the wing θ_1 the downwash on the wing is given by:

$$w(\theta_1) = \frac{1}{4\pi} \int_0^\pi \frac{\frac{\partial \Gamma}{\partial \theta} d\theta}{y_1 - y} \tag{2}$$

therefore

$$w(\theta_1) = u_\infty \sum_{n=1}^{\infty} nA_n \frac{\sin n\theta_1}{\sin \theta_1} \tag{3}$$

Since θ_1 is chosen to be any arbitrary point, equation 3 holds for a general point θ, hence

$$w \sin\theta = u_\infty \sum_{n=1}^{\infty} nA_n \sin n\theta \tag{4}$$

The downwash velocity creates an induced angle α_i at a given wing location which relates the geometric angle of attack α and the real angle α_0, by:

$$\begin{aligned} \alpha_0(y) &= \alpha(y) - \alpha_i(y) \\ \alpha_0(y) &= \alpha(y) - \frac{w(y)}{u_\infty} \end{aligned} \tag{5}$$

[a]the circulation distribution shown in figure 1 is a general circulation distribution that can be defined by lifting-line theory, whereas the VG circulation distribution is defined later

assuming a small induced angle. Furthermore, assuming that the true angle of attack of the wing section is small then the lift is linearly related to the angle using the lift curve slope a_0 by $c_l = \alpha_0 a_0$. The Kutta-Joukowski theorem, which relates lift to circulation, is given by $c_l = 2\Gamma/cu_\infty$ for an aerofoil with chord c. Equations 1 and 4 can then be substituted into equation 5 to obtain:

$$\sum_{n=1}^{\infty} A_n \sin n\theta(\mu n + \sin\theta) = \mu\alpha \sin\theta \tag{6}$$

where $\mu = a_0 c/8s$. Equation 6 allows the calculation of the coefficients given the wing's geometric properties.

The lift and induced drag of the wing can be obtained using Kutta-Joukowski theorem assuming the induced angle is small:

$$L = \int_{-s}^{s} \rho u_\infty \Gamma dy \quad , \quad D_i = L\frac{w}{u_\infty} = \int_{-s}^{s} \rho u_\infty \Gamma \frac{w}{u_\infty} dy \tag{7}$$

The circulation shed at the wing tip can be approximated as being the maximum value of the circulation. For this scenario, circulation distribution is approximated using only the first sine term of the series, hence only A_1 needs to be found. Using the first term will create a symmetric distribution, where the maximum value is at $\theta = \pi/2$. Using this fact, and $n = 1$ in equation 6, gives $A_1 = \mu\alpha/(\mu + 1)$. If $a_0 = 2\pi$, from equation 1, the maximum circulation is then given by:

$$\Gamma_{max} = \frac{u_\infty \pi c \alpha}{\mu + 1} \tag{8}$$

III.B. Extended Lifting-Line for VG Geometry

The geometry and scale of a typical VG means that the flow in the boundary layer becomes an important aspect of the total flow. Furthermore the VG has a much lower aspect ratio than a typical aircraft wing. The model developed here for predicting the strength of the shed vortex uses the lifting-line theory described above as a basis, with extra elements added to more fully capture the physics of the problem.

The structure of the aerodynamic body being modelled is shown in figure 2. It is a thin rectangular VG of length l and height h, where the vertical location on the VG is given by z. The VG is mounted on a flat plate and is inclined to the freestream flow at an angle α.

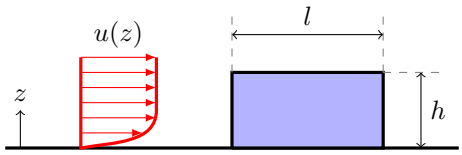

Figure 2: Schematic of vortex generator geometry

The local flow at the VG includes the boundary layer profile. It is important to include the boundary layer as the VG may either be immersed within the boundary layer, or will have a significant fraction of its total height within the boundary layer. For most flows, a turbulent boundary layer is a reasonable assumption, which has a height δ, and has a profile given by a turbulent boundary layer power law (where typically $n = 9$):

$$u(z) = \begin{cases} u_e(z/\delta)^{1/n} & z < \delta \\ u_e & z \geq \delta \end{cases}$$

where u_e is the local freestream velocity (or the boundary layer edge velocity at the VG).

A single VG can be considered as one half of a lifting wing hence there is always a mirror pair of VGs that make up a whole wing. The wing geometry is transformed to the VG geometry such that the wing semi-span is now the height of the VG h, and the spanwise location along the wing is given by the vertical height away from the surface z. Therefore, the wing is of total span $2h$, and $-h \leq z \leq h$. For the lifting-line theory, this is transformed so that $0 \leq \theta \leq \pi$, hence the vertical coordinate is transformed by $z = -h\cos\theta$. The velocity profile then becomes:

$$u(\theta) = \begin{cases} u_e(-\frac{h\cos\theta}{\delta})^{1/n} & -h\cos\theta < \delta \\ u_e & -h\cos\theta \geq \delta \end{cases} \tag{9}$$

To calculate the circulation distribution over the whole wing (i.e. the VG and its pair), the lifting-line theory is used as a basis. However, this theory assumes that the wing has a high aspect ratio, which VGs tend not to have. The implication of a low aspect ratio wing is that the vortex which forms along the length of the VG has a significant impact on the overall flow on the VG. The circulation distribution can therefore no longer be approximated by a lifting-line alone. Instead, an additional component of the circulation must be added, and this is due to the vortex. The additional component comes from the leading-edge suction theory of Polhamus,[33,34] which is a theory to add in the extra lift created by the vortex which rolls along the leading edge of delta wings. Hence, the total circulation shed from the wing is given by:

$$\Gamma = \Gamma_p + \Gamma_v \tag{10}$$

where the subscripts p and v represent the potential (or lifting-line) and vortex-lift parts of the circulation.

The potential component of the circulation comes from the lifting-line theory outlined above. A general, symmetric circulation distribution is given by an infinite sine series (equation 1), which is written in terms of the VG geometry as:

$$\Gamma(\theta) = 4hu(\theta)\sum_{n=1}^{\infty} A_n \sin(n\theta)$$

(for generality, the velocity is written as a function of the vertical location, however, this will be simplified later). The Fourier series must be truncated for computational purposes. Once the series is truncated to a finite number of Fourier coefficients, the coefficients are solved for by considering equation 1 at a number of vertical locations along the VG. The number of locations chosen must equal to number of coefficients hence a linear system of equations is formed which can then be solved. The coefficients are therefore calculated based solely on the geometry and angle of the VG. If, for example, the series is truncated to four coefficients, then equation 1 becomes:

$$A_1\sin\theta(\mu+\sin\theta) + A_3\sin 3\theta(3\mu+\sin\theta) + A_5\sin 5\theta(5\mu+\sin\theta) + A_7\sin 7\theta(7\mu+\sin\theta) = \mu\alpha\sin\theta \tag{11}$$

Only odd terms of the Fourier series are used as these form the symmetric circulation distribution required. Figure 3 shows the values for the coefficients when they are truncated to four terms for various values of h/l at $\alpha = 10°$. The vertical locations for evaluating equation 11 are linearly distributed along the span. The coefficients are normalised by A_1. The graphs show that the first term coefficient is much larger than the remaining coefficients (this trend continues when truncating with more terms). Furthermore, as long as the ratio of height to length is less than 1.0, which is common for a VG, then the value of A_3 is less than 5% of the value of A_1. This is further confirmed by figure 4, which is the circulation distribution using various levels of trunction of uniform oncoming flow. It shows that for typical VG values of h/l (i.e. less that 1.0), that the circulation distributions match very well. It is therefore reasonable to assume that for typical VG geometries, taking only the first term is sufficient.

Taking only the first term of the series results in a sine circulation distribution over the wing, hence:

$$\Gamma_p(\theta) = 4hu(\theta)A_1\sin\theta \tag{12}$$

The coefficient is obtained from setting $n = 1$ in equation 6, so:

$$A_1 = \mu\alpha/(\mu+\sin\theta) \tag{13}$$

where $\mu = al/8h$. The velocity is written as a function of the vertical location, however, lifting line theory does not allow this. To obtain a constant oncoming velocity, the velocity distribution over the VG is averaged. Equation 12 then becomes:

$$\Gamma_p(\theta) = \frac{4h\mu\alpha\bar{u}\sin\theta}{\mu+\sin\theta} \tag{14}$$

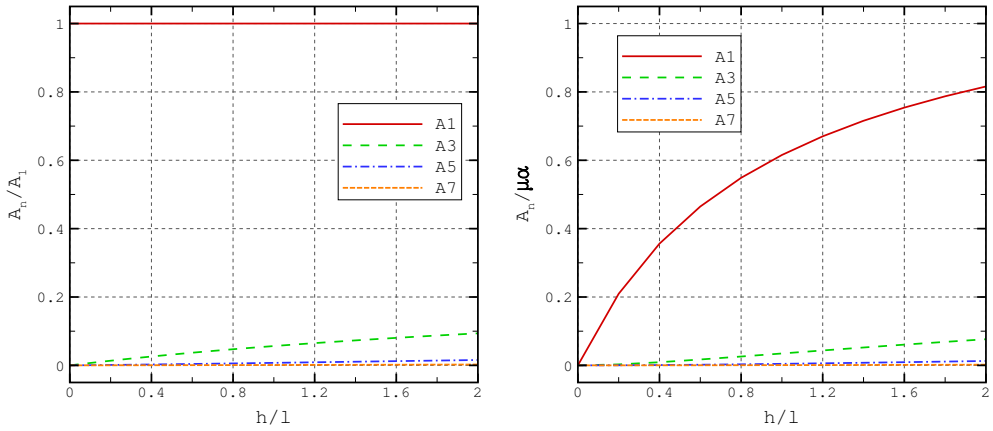

(a) Normalised values (b) Raw values

Figure 3: Values of coefficients for truncating with four terms

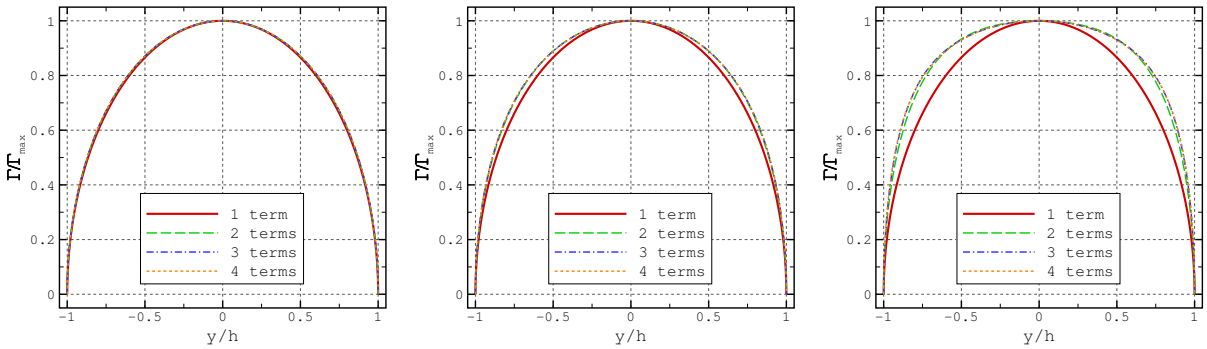

(a) $h/l = 0.1$ (b) $h/l = 0.5$ (c) $h/l = 2.0$

Figure 4: Lifting-line circulation distributions after truncating with 1, 2, 3 and 4 terms

where $\bar{u}$ is the span-averaged velocity. Equation 14 is then integrated over the span to give the total shed circulation and this value used in equation 10.

The vortex-lift component comes from Polhamus' leading edge suction theory.[33,34] This is due to the vortex rolling up along the length of the VG and causing an additional component of lift. The suction theory is derived for a delta wing which has a leading edge angle of Λ, however, we have a rectangular VG so the angle of the edge that the vortex rolls along (the tip of the VG in this case) is zero.

The lift coefficient for the suction theory is given as:

$$c_{l_v} = K_v \frac{\cos\alpha \sin^2\alpha}{\cos\Lambda} \tag{15}$$

where K_v is a constant, which for aspect ratios less than four is very close to π. Given a lift coefficient, the circulation value may be calculated using $\Gamma = \frac{1}{2}\bar{u}cC_L$ (which is obtained by equating the Kutta-Joukowski theorem with the lift equation). The circulation due to the vortex lift is therefore given by:

$$\Gamma_v = \frac{1}{2}\bar{u}l\pi \cos\alpha \sin^2\alpha \tag{16}$$

The total circulation distribution is then found by substituting equations 16 and 14 into equation 10.

III.C. Validation

To validate the circulation model, a set of experimental data from Wendt[28] was used. This data contains 59 different tests of rectangular vortex generators with varying lengths, heights and angles. The experiments were all undertaken at incompressible velocities, with Reynolds numbers of the order of 1.0×10^6. The downstream flowfield was probed to obtain velocity data, and from this, circulation data was reconstructed. For this data, the aspect ratio is defined as being $AR = 8h/\pi c$, so this definition is used in this section.

The analytical model is compared to two other models. The first is the basic lifting-line model as given in equation 8. The second is a model described by Wendt, and is given as:

$$\Gamma = \frac{k_1 u_e \alpha l}{1 + \frac{k_2 \pi l}{8h}} \tanh \left[k_3 \left(\frac{h}{\delta} \right)^{k_4} \right]$$

The model is a slight recasting of the Prandtl model, where the hyperbolic tangent function is used to represent the influence of the boundary layer. The constants in the model are obtained by performing a least squares regression to the experimental circulation results obtained by Wendt. These constants are:

$$k_1 = 1.61 \quad , \quad k_2 = 0.48 \quad , \quad k_3 = 1.41 \quad , \quad k_4 = 1.00$$

The three models being compared are therefore a simple model containing a limited amount of physics (Prandtl model), a more complicated model that augments the Prandtl model with an empirical fit (Wendt model) and a more complicated, but still analytical, model with more physics to represent the problem being approximated (developed in this paper). Table 1 shows the full matrix of experimental tests performed and the results of the model predictions.

A statistical summary of the results from table 1 are shown in table 2 and also graphically as a box-plot in figure 5 to show the ranges of the data. Table 2 shows that the average error between the models and the experimental data is, overall, the lowest with the newly developed model. Furthermore, the overall range, the inter-quartile range and the median solution are all lowest with the newly developed model. This indicates that most of the data points of the newly developed model are very close to the experimental data compared to the other two models.

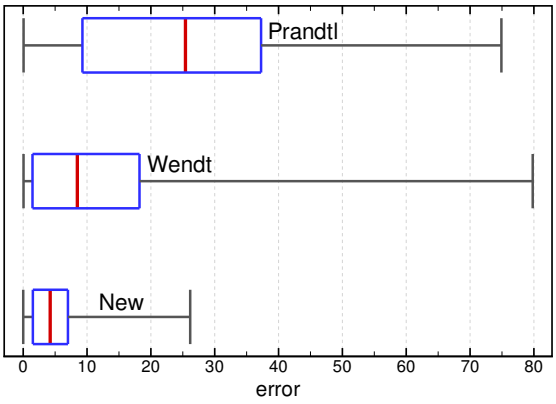

Figure 5: Boxplot of circulation model validation.

Table 1: Circulation validation results

						Γ				Error		
#	α	l	h	h/δ	u_e	Exp.	New	Wendt	Prandtl	New	Wendt	Prandtl
	deg	mm	mm		m/s	m^2/s	m^2/s	m^2/s	m^2/s	%	%	%
1	8	40.6	10.2	0.57	85	0.291	0.278	0.295	0.367	-4.6	1.5	26.1
2	12	40.6	10.2	0.57	85	0.471	0.475	0.443	0.550	0.9	-6.0	16.8
3	16	40.6	10.2	0.57	85	0.643	0.706	0.590	0.734	9.8	-8.2	14.1
4	20	40.6	10.2	0.57	85	0.940	0.963	0.738	0.917	2.5	-21.5	-2.4
5	16	40.6	10.2	0.57	85	0.722	0.706	0.590	0.734	-2.2	-18.2	1.6
6	16	40.6	10.2	0.62	129	1.149	1.081	0.946	1.114	-5.9	-17.6	-3.1
7	16	40.6	10.2	0.65	187	1.724	1.576	1.412	1.614	-8.6	-18.1	-6.4
8	16	8.5	2.1	0.12	85	0.153	0.124	0.031	0.152	-19.3	-79.8	-0.9
9	16	8.5	5.1	0.29	85	0.240	0.183	0.096	0.275	-23.6	-60.1	14.4
10	16	8.5	10.2	0.57	85	0.253	0.236	0.187	0.383	-6.8	-26.1	51.4
11	16	8.5	15.2	0.86	85	0.297	0.266	0.246	0.440	-10.5	-17.1	48.3
12	16	8.5	20.3	1.14	85	0.307	0.286	0.278	0.477	-6.9	-9.5	55.4
13	16	13.6	2.8	0.19	85	0.223	0.195	0.071	0.211	-12.6	-68.2	-5.5
14	16	13.6	5.1	0.29	85	0.342	0.253	0.134	0.328	-26.2	-60.8	-4.2
15	16	13.6	8.1	0.46	85	0.315	0.308	0.225	0.437	-2.1	-28.5	38.9
16	16	13.6	10.2	0.57	85	0.315	0.337	0.277	0.495	7.0	-12.2	57.3
17	16	13.6	15.2	0.86	85	0.429	0.389	0.372	0.596	-9.3	-13.2	38.8
18	16	13.6	16.3	0.91	85	0.419	0.397	0.385	0.613	-5.2	-8.1	46.2
19	16	13.6	20.3	1.14	85	0.485	0.425	0.426	0.665	-12.4	-12.2	37.0
20	16	13.6	25.4	1.43	85	0.428	0.451	0.456	0.714	5.3	6.5	66.8
21	16	13.6	30.5	1.71	85	0.476	0.469	0.472	0.751	-1.5	-0.9	57.8
22	16	13.6	35.6	2.00	85	0.446	0.483	0.481	0.780	8.3	7.9	74.9
23	16	20.3	5.1	0.29	85	0.322	0.327	0.172	0.367	1.7	-46.7	13.9
24	16	20.3	10.2	0.57	85	0.435	0.447	0.376	0.591	2.9	-13.6	35.8
25	16	20.3	12.2	0.69	85	0.493	0.483	0.443	0.656	-2.1	-10.2	33.1
26	16	20.3	15.2	0.86	85	0.552	0.526	0.519	0.739	-4.6	-6.0	33.8
27	16	20.3	20.3	1.14	85	0.596	0.584	0.602	0.848	-2.0	1.1	42.3
28	16	20.3	24.4	1.37	85	0.667	0.618	0.643	0.916	-7.3	-3.6	37.3
29	16	25.4	5.1	0.29	85	0.450	0.378	0.194	0.386	-16.0	-56.9	-14.3
30	16	25.4	6.4	0.36	85	0.421	0.420	0.260	0.460	-0.2	-38.3	9.3
31	16	25.4	10.2	0.57	85	0.525	0.520	0.440	0.641	-0.9	-16.2	22.1
32	16	25.4	15.2	0.86	85	0.626	0.618	0.618	0.819	-1.2	-1.2	30.8
33	16	25.4	20.3	1.14	85	0.719	0.691	0.725	0.955	-3.9	0.8	32.9
34	16	25.4	25.4	1.43	85	0.781	0.746	0.788	1.061	-4.5	0.9	35.8
35	16	25.4	30.5	1.71	85	0.825	0.786	0.826	1.145	-4.7	0.1	38.8
36	16	25.4	35.6	2.00	85	0.862	0.819	0.850	1.214	-5.0	-1.4	40.8
37	16	25.4	45.7	2.57	85	0.866	0.866	0.877	1.319	-0.0	1.3	52.3
38	16	30.5	5.1	0.29	85	0.399	0.425	0.212	0.399	6.5	-46.8	0.1
39	16	30.5	7.6	0.43	85	0.530	0.512	0.359	0.548	-3.3	-32.2	3.4
40	16	30.5	10.2	0.57	85	0.591	0.587	0.497	0.679	-0.7	-16.0	14.9
41	16	30.5	15.2	0.86	85	0.704	0.702	0.708	0.883	-0.3	0.6	25.4
42	16	30.5	18.3	1.03	85	0.776	0.758	0.795	0.985	-2.3	2.4	26.9
43	16	30.5	20.3	1.14	85	0.817	0.790	0.838	1.043	-3.4	2.6	27.7
44	16	30.5	36.6	2.06	85	0.985	0.955	1.001	1.375	-3.1	1.7	39.6
45	16	35.6	5.1	0.29	85	0.451	0.470	0.228	0.410	4.2	-49.5	-9.2
46	16	35.6	8.9	0.50	85	0.662	0.609	0.471	0.641	-8.0	-28.8	-3.2
47	16	35.6	10.2	0.57	85	0.648	0.649	0.547	0.710	0.1	-15.6	9.5
48	16	35.6	15.2	0.86	85	0.780	0.779	0.790	0.935	-0.1	1.3	19.9
49	16	35.6	20.3	1.14	85	0.944	0.881	0.944	1.117	-6.7	-0.1	18.3
50	16	35.6	21.3	1.20	85	0.941	0.898	0.967	1.148	-4.6	2.7	22.0
51	16	35.6	42.7	2.40	85	1.170	1.123	1.173	1.604	-4.0	0.3	37.1
52	16	40.6	5.1	0.29	85	0.429	0.513	0.240	0.417	19.5	-43.9	-2.7
53	16	40.6	10.2	0.57	85	0.713	0.706	0.590	0.734	-1.0	-17.2	2.9
54	16	40.6	15.2	0.86	85	0.824	0.850	0.864	0.977	3.2	4.9	18.6
55	16	40.6	20.3	1.14	85	0.961	0.964	1.040	1.178	0.4	8.2	22.5
56	16	40.6	24.4	1.37	85	1.044	1.038	1.133	1.312	-0.6	8.5	25.7
57	16	40.6	25.4	1.43	85	1.045	1.054	1.151	1.342	0.8	10.1	28.5
58	16	40.6	30.5	1.71	85	1.210	1.124	1.221	1.480	-7.1	0.9	22.3
59	16	40.6	35.6	2.00	85	1.243 ±5%	1.181	1.268	1.597	-5.0	2.0	28.5

Table 2: Statistical results of circulation validation

	New	Wendt	Prandtl
Mean absolute error	5.6%	16.9%	26.3%
Max absolute error	26.2%	79.8%	74.9%
Min absolute error	0.0%	0.1%	0.1%
St. Dev. absolute error	5.6%	19.6%	18.1%

Figure 6 gives plots of the effect of varying α, AR and h/δ on the circulation values from the experimental data and the three models. The remaining parameters are kept fixed. It can be seen that, as before, the new model produces values that fit the experimental data better than the basic Prandtl model, and also better than the empirical model that was fit to this data by Wendt. This emphasises the importance of the extra physics in the analytical model, but also demonstrates that an analytical model is sufficient to predict the strength of a shed vortex from VGs.

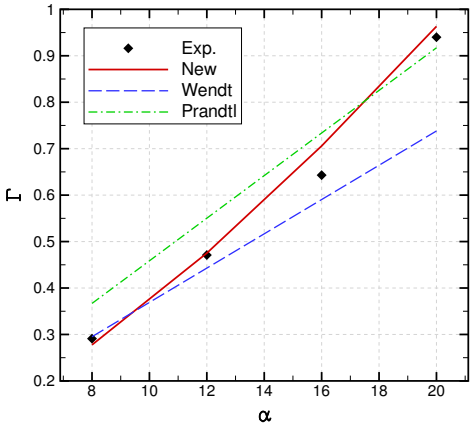

(a) Varying α, AR=0.64, h/δ=0.57

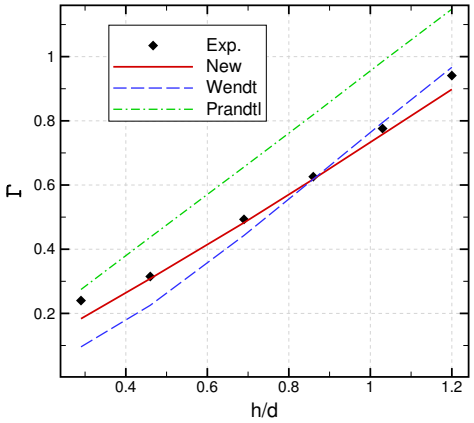

(b) Varying h/δ, AR=1.53, α=16

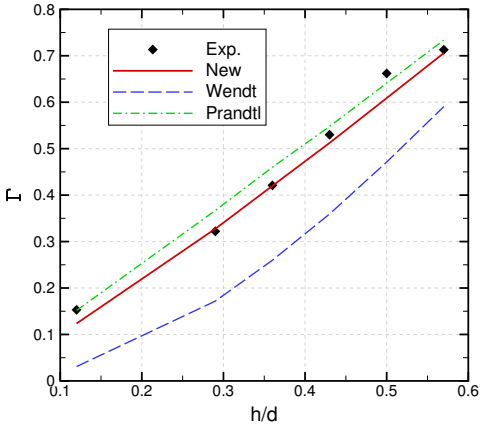

(c) Varying h/δ, AR=0.64, α=16

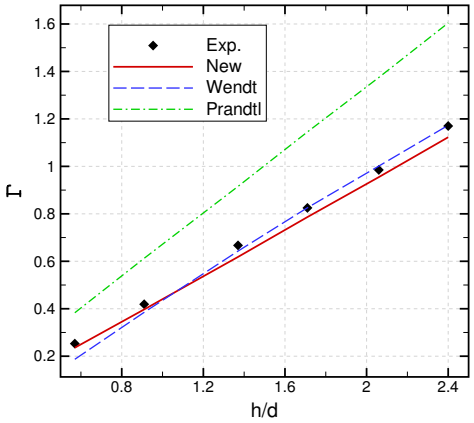

(d) Varying h/δ, AR=3.06, α=16

Figure 6: Comparison graphs of experimental data with models

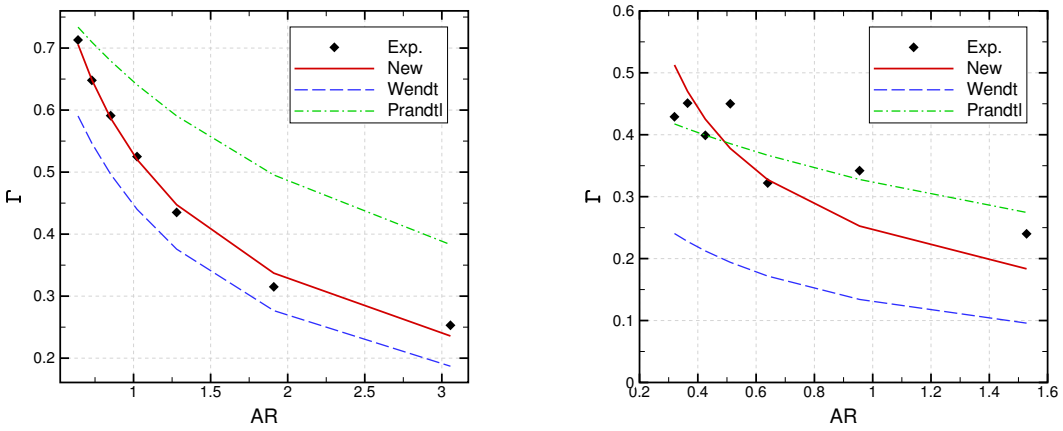

(a) Varying AR, h/δ=0.57, α=16

(b) Varying AR, h/δ=0.29, α=16

(c) Varying AR, h/δ=0.86, α=16

(d) Varying AR, h/δ=1.14, α=16

Figure 6 (Cont.): Comparison graphs of experimental data with models

IV. Source Term Modelling

The extended lifting-line approach, which uses traditional lifting-line methods with vortex lift modifications, for modelling the strength of shed vortices has been shown to be particularly effective at modelling the strength of the shed vortices. In this section, the development of the circulation model into a source term CFD approach is presented. The source term method, of which the BAY model[8] is the most common, alleviates the issues around meshing by using source terms in cells where the VG that the source term is representing would otherwise be. The new model is implemented in a conceptually similar way to the BAY model.

IV.A. BAY Model

The BAY model simulates the lift force acting on the flow due to the VG. Hence vorticity is induced that depends on the VG geometry and local flow variables. The lifting source term, $\mathbf{S}_i$, acts on grid point i. The term is added to the right hand side of the equations, so in a finite volume flow solver, the momentum equation becomes:

$$V_i \frac{\Delta(\rho \mathbf{u})_i}{\Delta t} = \sum_j \mathbf{F}_{M_j} A_j + \mathbf{S}_i$$

where

$$\mathbf{S}_i = C_{VG} A_{VG} \frac{V_i}{\sum V_i} \alpha \rho |\mathbf{u}|^2 \hat{\mathbf{l}}$$

where C_{VG} is a tunable constant, A_{VG} is the vortex generator area, V_i is the volume of the cell, $\sum V_i$ is the total volume of the cells that the source term is applied to and $\hat{\mathbf{l}}$ is the unit vector on which the side force acts.

The VG is described by three unit vectors, as shown in figure 7, where $\hat{\mathbf{b}}$ is along the VG span, $\hat{\mathbf{t}}$ is along the VG length and $\hat{\mathbf{n}}$ is normal to the VG surface. These three vectors form an orthonormal system. Using small angle approximations, and introducing the term $(\hat{\mathbf{u}} \cdot \hat{\mathbf{t}})$ which is used to simulate loss of lift at higher VG angles, the lift force can be written in terms of the three defining vectors:

$$\mathbf{S}_i = C_{VG} A_{VG} \frac{V_i}{\sum V_i} \rho (\mathbf{u} \cdot \hat{\mathbf{n}})(\mathbf{u} \times \hat{\mathbf{b}})(\hat{\mathbf{u}} \cdot \hat{\mathbf{t}}) \tag{17}$$

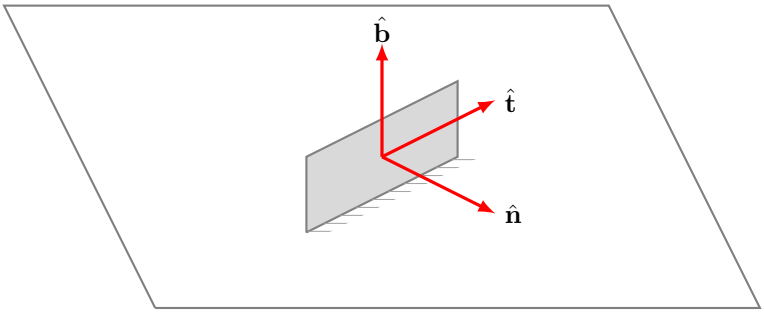

Figure 7: VG definition for BAY model

The empirical constant in equation 17 is often set based on user experience. Bender *et al.*[8] showed, however, that for values of $C_{VG} > 5$, that the change in the resulting lift force became negligible because the flow is forced to align itself with the VG such that the local angle of attack approaches zero. Careful consideration of the constant is also needed for flow solver convergence. In general, a constant of 10 is a good choice.[35]

IV.B. New Model

The new vortex generator model is implemented in a conceptually similar manner to the BAY model, where a forcing term is added to the right hand side of the equations in certain cells, and this is a function of some ratio of the size of the cells to the total size of the cells used. However, the formulation that results from manipulating the circulation model developed in this paper leads to a model without the need to empirically consider a constant that results in different solutions depending on its value.

The new model also requires a resultant force to be added. This force is due to the lift from the VG and its drag also. The lift of the VG, like the circulation, is due to the potential component L_p and the vortex lift component L_v:

$$\begin{aligned} L &= L_p + L_v \\ &= \frac{1}{2} \rho \overline{|\mathbf{u}|}^2 lh (C_{L_p} + C_{L_v}) \end{aligned}$$

where $\overline{|\mathbf{u}|}$ is the span-averaged absolute velocity vector which is a general form used in the simple circulation model. The general form is used to account for the simulation having non-zero values for spanwise and vertical velocities. The potential lift coefficient comes from the potential circulation value (which is the integrated form of equation 14) and the vortex lift coefficient comes from Polhamus,[33] leading to an expression for the total lift of the VG as:

$$L = \frac{1}{2}\rho\overline{|\mathbf{u}|}^2 lh\left(\frac{2\Gamma_p}{\overline{|\mathbf{u}|}l} + \pi\cos\alpha\sin^2\alpha\right) \tag{18}$$

The drag of the VG is also due to the potential component D_p and the vortex lift component D_v:

$$\begin{aligned} D &= D_p + D_v \\ &= \frac{1}{2}\rho\overline{|\mathbf{u}|}^2 lh(C_{D_p} + C_{D_v}) \end{aligned}$$

The potential drag is given by the induced drag only, and is defined sectionally:

$$C_{d_p} = C_{d_i} = C_{l_p}\tan(\alpha_i) = C_{l_p}\tan\left(\tan^{-1}\left(\frac{w}{u}\right)\right) = C_{l_p}\frac{w}{u}$$

where w is the induced velocity and is given by equation 4. As noted previously, the first term in the series is sufficient to model the circulation of the VG. A_1 is given by equation 13, hence:

$$\frac{w}{u} = \frac{\mu\alpha}{\mu + \sin\theta}$$

therefore:

$$C_{d_p} = C_{l_p}\frac{\mu\alpha}{\mu + \sin\theta} = \frac{2\Gamma_p}{\overline{|\mathbf{u}|}l}\frac{\mu\alpha}{(\mu + \sin\theta)} \tag{19}$$

which is integrated over the VG span to evaluate C_{D_p}. The vortex component of the drag is due to Polhamus:[34]

$$C_{D_v} = C_{L_v}\tan\alpha = \pi\cos\alpha\sin^2\alpha\tan\alpha \tag{20}$$

Hence the overall lift and drag forces on the VG are available. The resultant vector is the total force vector acting on the flow due to the VG, and assuming L acts in a purely spanwise direction and D acts in a purely streamwise direction (as shown in figure 8), is given by:

$$\mathbf{S} = \begin{pmatrix} L \\ D \\ 0 \end{pmatrix} \tag{21}$$

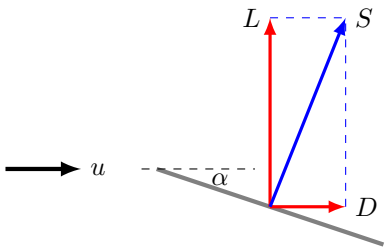

Figure 8: Overall force components acting on VG

The overall force is split over each cell as per the BAY model:

$$\mathbf{S}_i = \frac{V_i}{\sum V_i}\mathbf{S} \tag{22}$$

V. Computational Results

Results of the new source term model for predicting VG flows is examined here. As an initial study, a flat-plate test case is considered that has experimental data associated with it. The new model is compared to fully-gridded CFD and the conventional BAY model.

V.A. Run Details

The test case considered is from the work of Yao *et al.*[36] The set-up consists of an isolated VG mounted on a flat plate in subsonic turbulent flow ($u_\infty = 34$m/s). A low profile (or sub-boundary layer) VG that has $h/\delta = 0.2$ is tested at an angle of $\alpha = 16°$. The VG has geometry of $h = 7$mm and $l = 49$mm and is shown in figure 9.

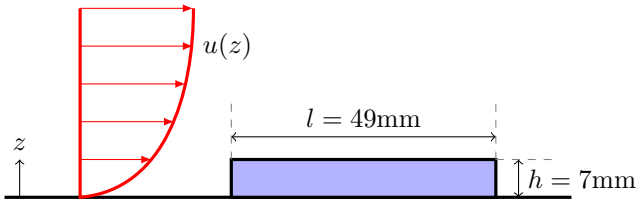

Figure 9: Schematic of vortex generator geometry for test

In the experiment, digital particle image velocimetry (PIV) measurements were taken to obtain flowfield slices at points downstream of the VG. These were then used to reconstruct circulation values at those slices downstream.

V.B. Simulation Framework

The capture of the important physics in flows around VGs involves using high quality, high density numerical meshes, with a suitable viscous solver. Both are required to capture the strength of the vortex, its convection downstream and its dissipation due to viscous effects. As such, a simulation framework has been developed that uses OpenFOAM[b] with high quality numerical meshes.

V.B.1. OpenFOAM

The solver package used in the current work is the open source CFD software OpenFOAM. The flow solver, with RANS turbulence modelling, is a unstructured solver based upon the SIMPLE algorithm (Semi-Implicit Method for Pressure-Linked Equations), which is an iterative procedure to solve the Navier-Stokes equations for steady-state problems. This iterative procedure, as originally implemented in OpenFOAM, relies on basic residual checking for steady state convergence criteria. After modification, steady state convergence is assessed using the standard deviation of the force coefficients. The turbulence model used was the standard Spalart-Allmaras (SA) model as defined by NASA Langley's Turbulence Modelling Resource[c], and has the minimum limiter of $0.3 \times \Omega$ for $\hat{S}$.

V.B.2. Meshes

The domain is specified to simulate an isolated vortex generator. The VG is mounted on a flat plate that is 4m long and 3m wide. The inlet boundary condition is 20m upstream of the leading edge of the flat plate and the outlet boundary is 16m downstream of the trailing edge of the flat plate. The height of the overall field is 20m. The geometry is shown in figure 10. A structured grid is constructed that has 97 grid points upstream and 97 grid points downstream of the flat plate, which has 385 points along its length. The domain has 129 points along the width and 129 vertically, resulting in approximately 9.6 million grid points. This is then converted to the unstructured format required by OpenFOAM and a farfield mesh reduction strategy is used to reduce the mesh down to 6.4 million points.

[b] `http://www.OpenFOAM.org/`
[c] `http://turbmodels.larc.nasa.gov`

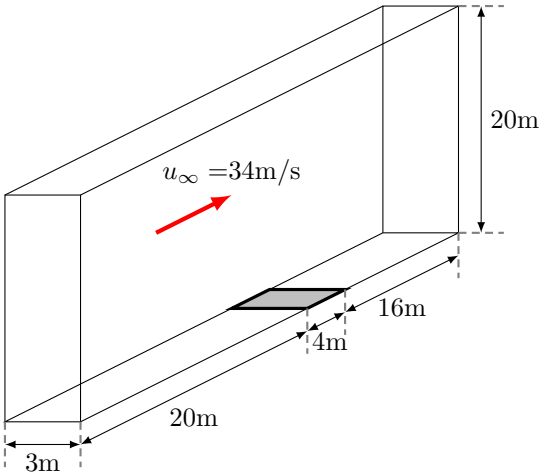

Figure 10: Computational domain

For the full CFD, the VG is modelled using a plane of faces using solid surface boundary conditions. The BAY model and new source term model are applied using cell tagging where the VG would effectively be. This means that the same meshes can be used for all of the three cases ensuring continuity in the results.

V.C. Results

The circulation decay downstream of the VG is shown in figure 11 for the three models compared to the experimental data. It is clear that all three of the modelling approaches have generally matched the trend of the circulation decay well. Close to the VG, it is perhaps apparent that the new model has matched both the fully gridded CFD and the experimental data slightly better than the BAY model, which appears to under predict circulation. Further downstream, the difference becomes negligible.

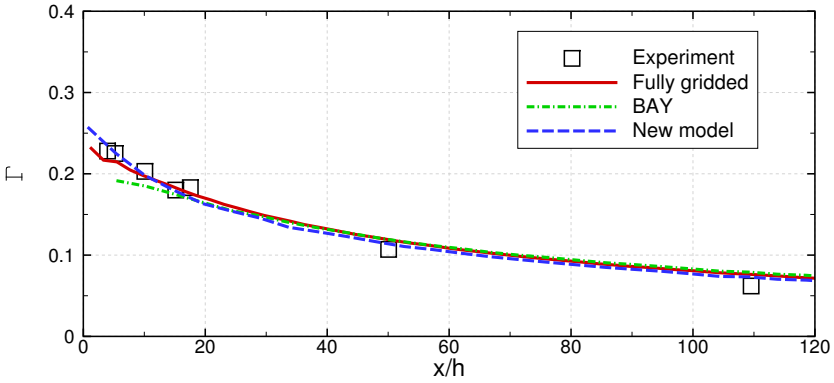

Figure 11: Circulation downstream of VG

Figure 12 shows contours of the axial velocities at a number of stations downstream of the VG corresponding to where experimental PIV data was taken. Again, good agreement between the modelling approaches is shown. The new model captures the important physics in the system, showing good dissipation due to viscosity and convection of the vortex downstream. Both the approximate vertical and spanwise locations of the vortex centre are captured accurately by the new model also.

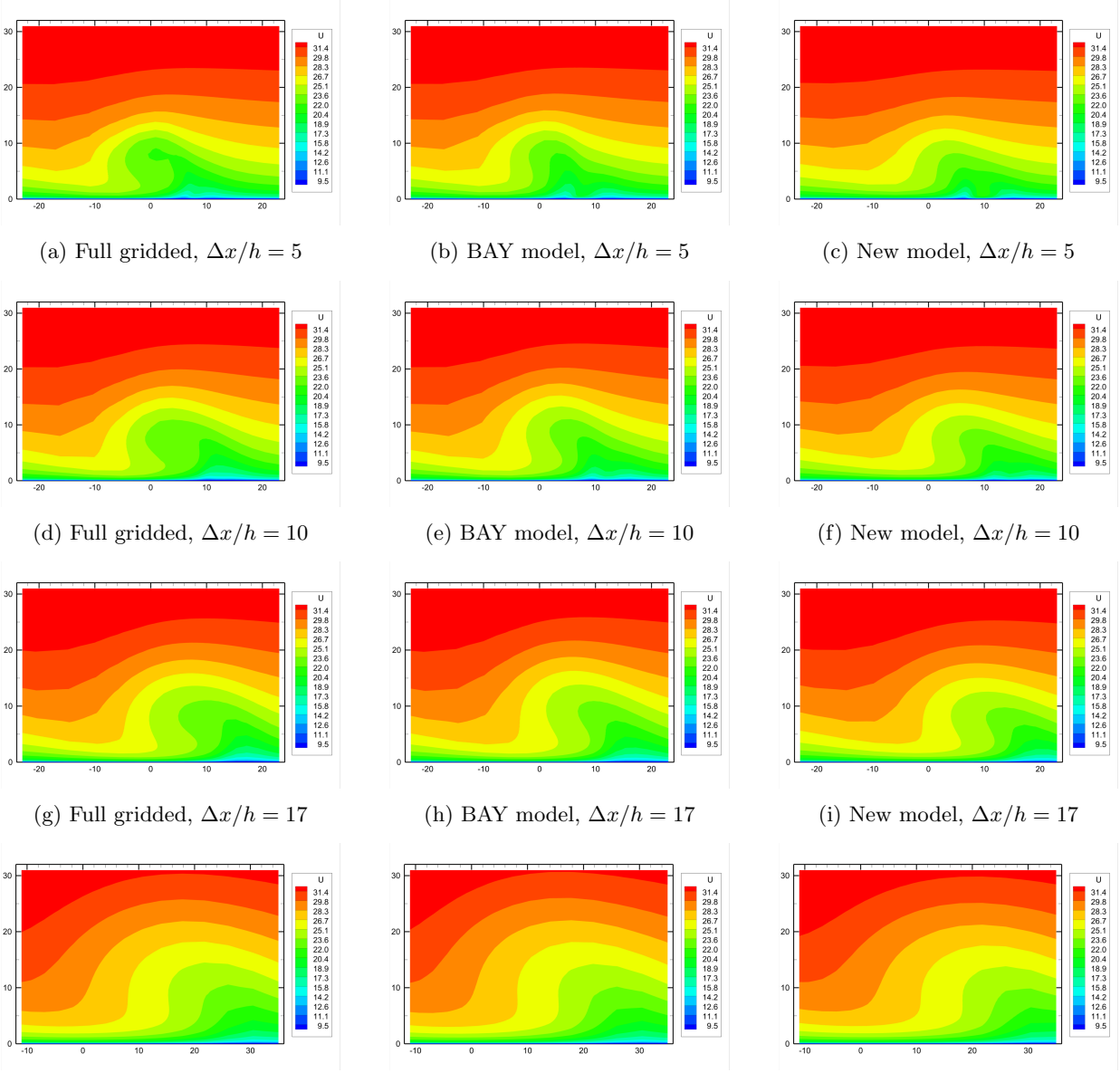

(a) Full gridded, $\Delta x/h = 5$ (b) BAY model, $\Delta x/h = 5$ (c) New model, $\Delta x/h = 5$

(d) Full gridded, $\Delta x/h = 10$ (e) BAY model, $\Delta x/h = 10$ (f) New model, $\Delta x/h = 10$

(g) Full gridded, $\Delta x/h = 17$ (h) BAY model, $\Delta x/h = 17$ (i) New model, $\Delta x/h = 17$

(j) Full gridded, $\Delta x/h = 50$ (k) BAY model, $\Delta x/h = 50$ (l) New model, $\Delta x/h = 50$

Figure 12: Axial velocity contours at downstream stations

VI. Conclusions

A new, physics-based model for simulating the effect of a vortex generator has been presented in this paper. An extended and modified lifting-line approach has been taken to model the strength of the shed vortex. Leading edge suction theory was used to mimic the effect of the vortex on the lift and the boundary layer has also been accounted for. The circulation model validates exceptionally well with a large suite of experimental data, showing a mean error of 5%, which is approximately the error in the experimental validation data, indicating excellent correlation.

This circulation model has then been used as a source term approach within a CFD framework to analyse the effect of the vortex on a flowfield. A flat plate test case was considered and the new model correlates well with experimental data and fully-gridded CFD. It also compares favourably with the commonly used BAY source term model, perhaps increasing the vortex capture in the immediate downstream flow behind the VG.

Acknowledgements

The authors would like to thank David Tring and Nigel Scrase of AgustaWestland, for their support of and contribution to this work. The financial support, via the HiPerTilt project, of AgustaWestland and Innovate UK (Technology Strategy Board) is also gratefully acknowledged.

References

[1]M. B. Bragg and G. M. Gregorek. Experimental study of airfoil performance with vortex generators. *Journal of Aircraft*, 24(5):305–309, 1987.

[2]M. Kerho, S. Hutcherson, R. F. Blackwelder, and R. H. Liebeck. Vortex generators used to control laminar separation bubbles. *Journal of Aircraft*, 30(3):315–319, 1993.

[3]J. C. Lin, S. K. Robinson, R. J. McGhee, and W. O. Valerezo. Separation control on high-lift airfoils via micro-vortex generators. *Journal of Aircraft*, 31(6):1317–1323, 1994.

[4]B. L. Storms and C. S. Jang. Lift enhancement of an airfoil using a gurney flap and vortex generators. *Journal of Aircraft*, 31(3):542–547, 1994.

[5]M.D. Weiberg, J.A. Maisel. Wind-tunnel tests of the XV-15 tilt rotor aircraft. Technical Report TM 81177, NASA.

[6]J. C. Lin. Review of research on low-profile vortex generators to control boundary-layer separation. *Progress in Aerospace Sciences*, 38(4–5):389–420, 2002.

[7]S. Shahunfar, S. S. Sattarzadeh, J. H. M. Fransson, and A. Talamelli. Revival of classical vortex generators now for transition delay. *Physical Review Letters*, 109(7):074501, 2012.

[8]E. E. Bender, B. H. Anderson, and P. J. Yagle. Vortex generator modeling for Navier-Stokes codes. In *American Society of Mechanical Engineers*, 1999. FEDSM 99-6929.

[9]B. G. Allan, C-S. Yao, and J. C. Lin. Numerical simulations of vortex generator vanes and jets on a flat plate. In *1st AIAA Flow Control Conference*, St Louis, Missouri, 2002. AIAA Paper 2002–3160.

[10]M. I. Yaras and A. D. Grosvenor. Evaluation of one- and two-equation low-Re turbulence models. part II–vortex-generator jet and diffusing s-duct flows. *International Journal for Numerical Methods in Fluids*, 42(12):1321–1343, 2003.

[11]E. Wik and S. T. Shaw. Numerical simulation of micro vortex generators. In *2nd AIAA Flow Control Conference*, Portland, Oregon, 2004. AIAA Paper 2004–2697.

[12]Q. Li and C. Liu. Declining angle effects of the trailing edge of a microramp vortex generator. *Journal of Aircraft*, 47(6):2086–2095, 2010.

[13]Y. Ito, M. Murayama, and K. Yamamoto. High-quality unstructured hybrid mesh generation for capturing effects of vortex generators. In *51st AIAA Aerospace Sciences Meeting including the New Horizons Forum and Aerospace Exposition*, Grapevine, Texas, 2013. AIAA Paper 2013–554.

[14]K. J. Forster and T. R. White. Numerical investigation into vortex generators on heavily cambered wings. *AIAA Journal*, 52(5):1059–1071, 2014.

[15]S. Lee, E. Loth, and H. Babinsky. Normal shock boundary layer control with various vortex generator geometries. *Computers and Fluids*, 49(1):233–246, 2011.

[16]C. Memory, D. O. Snyder, and J. Bons. Numerical simulation of vortex generating jets in zero and adverse pressure gradients. In *46th AIAA Aerospace Sciences Meeting and Exhibit*, Reno, Nevada, 2008. AIAA Paper 2008–558.

[17]H. Shan, L. Jiang, C. Liu, M. Love, and B. Maines. Numerical study of passive and active flow separation control over a naca0012 airfoil. *Computers and Fluids*, 37(8):975–992, 2008.

[18]H. Chen, S. Kandasamy, S. Orszag, R. Shock, S. Succi, and V. Yakhot. Extended boltzmann kinetic equation for turbulent flows. *Science*, 301(5633):633–636, 2003.

[19]B. Konig, E. Fares, and S. Nolting. Fully-resolved lattice-boltzmann simulation of vane-type vortex generators. In *7th AIAA Flow Control Conference*, Alanta, Georgia, 2014. AIAA Paper 2014–2795.

[20]W. G. Kunik. Application of a computational model for vortex generators in subsonic internal flows. In *AIAA/ASME/SAE/ASEE 22nd Joint Propulsion Conference*, Huntsville, Alabama, 1986. AIAA Paper 1986–1458.

[21]N. E. May. A new vortex generator model for use in complex configuration CFD solvers. In *19th AIAA Applied Aerodynamic Conference*, Anaheim, California, 2001. AIAA Paper 2001–2434.

[22]A. Jirasek. Vortex-generator model and its application to flow control. *Journal of Aircraft*, 42(6):1486–1491, 2005.

[23]JS. Yi, C. Kim, and B. J. Lee. Adjoint-based design optimization of vortex generator in an S-shaped subsonic inlet. *AIAA Journal*, 50(11):2492–2507, 2012.

[24]F. von Stillfried, S. Wallin, and A. V. Johansson. Vortex-generator models for zero- and adverse-pressure-gradient flows. *AIAA Journal*, 50(4):855–866, 2012.

[25]M. Kerho and B. Kramer. Enhanced airfoil design incorporating boundary layer mixing devices. In *41st AIAA Aerospace Sciences Meeting and Exhibit*, Reno, Nevada, 2003. AIAA Paper 2003–211.

[26]M. Drela. Xfoil: An analysis and design system for low reynolds number airfoils. In T. J. Mueller, editor, *Low Reynolds Number Aerodynamics*, pages 1–12. Springer Berlin Heidelberg, 1989.

[27]M. Drela and M.B. Giles. Viscous-inviscid analysis of transonic and low reynolds number airfoils. *AIAA Journal*, 25(10):1347–1355, 1987.

[28]B. J. Wendt. Parametric study of vortices shed from airfoil vortex generators. *AIAA Journal*, 42(11):2185–2195, 2004.

[29]J. C. Dudek. Empirical model for vane-type vortex generators in a navier–stokes code. *AIAA Journal*, 44(8):1779–1789, 2006.

[30]L. Prandtl. Applications of modern hydrodynamics to aeronautics. Technical report, NACA, 1923. NACA Report 116.

[31]H. Glauert. *The Elements of Aerofoil and Airscrew Theory*. Cambridge University Press, 1983.

[32]A. Pope. *Basic Wing and Airfoil Theory*. McGraw-Hill, 1951.

[33]E. C. Polhamus. A concept of the vortex lift of sharp-edge delta wings based on a leading-edge suction analogy. Technical report, NASA, 1966. NASA TN D-3767.

[34]E. C. Polhamus. Application of the leading-edge-suction analogy of vortex lift to the drag due to lift of sharp-edge delta wings. Technical report, NASA, 1968. NASA TN D-4739.

[35]J. C. Dudek. Modeling vortex generators in a Navier-Stokes code. *AIAA Journal*, 49(4):748–759, 2011.

[36]C-S. Yao, J. C. Lin, and B. G. Allan. Flow-field measurements of device-induced embedded streamwise vortex on a flat plate. In *1st AIAA Flow Control Conference*, St. Louis, Missouri, 2002. AIAA Paper 2002–3162.